Counterion Effects on the Intramolecular Electron-Transfer Rate of Mixed-Valence Biferrocenium Salts: Micromodulation and Phase Transitions

Teng-Yuan Dong, Takeshi Kambara,[1] and David N. Hendrickson*

Contribution from the School of Chemical Sciences, University of Illinois, Urbana, Illinois 61801. *Received December 2, 1985*

Abstract: The effect of changing the counterion from I_3^- to I_2Br^-, Br_2I^-, or PF_6^- upon the rate of *intra*molecular electron transfer in the mixed-valence biferrocenium cation is examined. Room temperature powder X-ray diffraction data are presented to show that the I_2Br^- and Br_2I^- salts are isostructural to biferrocenium triiodide. The 4.2 K X-band EPR spectrum of biferrocenium Br_2I^- is axial ($g_\parallel$ = 3.60 and $g_\perp$ = 1.75) and very similar to that for the I_3^- salt. However, the g-tensor anisotropy ($g_\parallel$ = 3.23 and $g_\perp$ = 1.90) observed for the 4.2 K EPR spectrum of biferrocenium I_2Br^- is appreciably reduced compared to that of the I_3^- and Br_2I^- salts. This probably reflects the low-symmetry environment provided by the asymmetric I-I-Br$^-$ anion. The ^{57}Fe Mössbauer characteristics of biferrocenium I_2Br^- resemble those of the I_3^- salt; however, everything is shifted to lower temperatures. The 150 K spectrum essentially consists only of two doublets (one Fe^{II} and one Fe^{III}). A third average-valence doublet grows in with increasing temperature until at ~340 K only this average doublet is seen. A temperature of only ~220 K is needed to give only an average-valence doublet for the Br_2I^- salt. Thus, replacing the I_3^- by the Br_2I^- anion leads to a dramatic reduction by ~150 deg in the temperature where the mixed-valence biferrocenium cation transfers an electron faster than the Mössbauer technique can sense. A qualitative model is developed to explain the effect of the anion replacement. The importance of the cation–cation and cation–anion interactions, as well as the intrinsic charge-oscillation barrier heights in the mixed-valence cations and anions, is discussed relative to the phase transition that is believed to be present in these compounds.

In very recent studies[2-7] it has been shown that the solid-state environment plays a crucial role in determining the rate of *intra*molecular electron transfer in various mixed-valence biferrocenium salts. Triiodide salts ($Y^- = I_3^-$) were studied. The

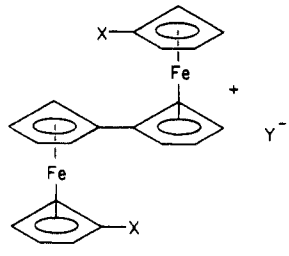

triiodide salts of the mixed-valence 1′,6′-dihalobiferrocenium cations (X = I, Br, or Cl) make up an interesting series. The X = I and Br compounds exhibit an *intra*molecular electron-transfer rate that is faster than the Mössbauer and EPR techniques can sense (i.e., faster than 10^{10} s^{-1}) from 300 K down to 4.2 K.[2,5,7-9] However, these two mixed-valence species do *not* have a delocalized electronic structure. That is, infrared spectra show the presence of both Fe^{II} and Fe^{III} moieties for each mixed-valence cation.[2,5] There is a potential-energy barrier in these X = I or Br biferrocenium salts. On the other hand, the rate of electron transfer is less than can be sensed by the Mössbauer technique (i.e., <10^7 s^{-1}) for the X = Cl analogue[5,9] which crystallizes with 0.5 mol of I_2 in addition to the I_3^- counterion. From X-ray structural results for the X = I[2,5] and Cl[5] triiodides it has been concluded that it is the positioning of the triiodide anion relative to the mixed-valence cation that controls the rate of *intra*molecular electron transfer in the cation. For the X = I and Br compounds the I_3^- anions are symmetrically disposed relative to the two iron ions in a given mixed-valence cation. Consequently, the ground-state double-well potential-energy surface is symmetric. The two vibronic states of the mixed-valence cation, $Fe_a^{II}Fe_b^{III}$ and $Fe_a^{III}Fe_b^{II}$, are at the same energy, and *intra*molecular electron transfer is relatively fast (tunneling?). The I_3^- anions in the X = Cl compound are not symmetrically disposed relative to the two iron ions in each cation. The Fe^{III} ion is on the average closer to the terminal charge-carrying iodine atoms of neighboring I_3^- anions. Thus, one vibronic state, say $Fe_a^{II}Fe_b^{III}$, is at appreciably lower energy than the other. As a result, the barrier for *intra*molecular electron transfer in the X = Cl cation is much larger than for the X = I, Br compounds.

Four 1′,6′-dialkylbiferrocenium triiodides (X = CH_2CH_3, $CH_2CH_2CH_3$, $CH_2CH_2CH_2CH_3$, and $CH_2C_6H_5$) have also been studied.[4,10] These four complexes give temperature-dependent Mössbauer spectra. At temperatures less than ~200 K, they each show two doublets, one for the Fe^{II} and the other for the Fe^{III} site. Increasing the sample temperature in each case leads to the two doublets moving together, eventually to become a single average doublet at temperatures of 275, 245, 275, and 260 K, respectively. X-ray structures have been reported at 298 and 110 K for the dipropyl compound[11] and at 363, 298, and 150 K for the di-*n*-butyl compound.[4] We suggested that the temperature dependence in electron transfer seen for these four compounds occurred as the result of the onset of motion in the solid state.[4,7] The motion could involve, in part, the triiodide ions interconverting between two configurations, one which can be described in a limiting form as $I_A^-\cdots I_B—I_C$ and the other as $I_A—I_B\cdots I_C^-$. In each configuration

(1) On sabbatical leave from the Department of Engineering Physics, The University of Electro-Communications, Chofu, Tokyo 182, Japan.
(2) Dong, T.-Y.; Cohn, M. J.; Hendrickson, D. N.; Pierpont, C. G. *J. Am. Chem. Soc.* **1985**, *107*, 4777.
(3) Cohn, M. J.; Dong, T.-Y.; Hendrickson, D. N.; Geib, S. J.; Rheingold, A. L. *J. Chem. Soc., Chem. Commun.* **1985**, 1095.
(4) Dong, T.-Y.; Hendrickson, D. N.; Iwai, K.; Cohn, M. J.; Rheingold, A. L.; Sano, H.; Motoyama, I.; Nakashima, S. *J. Am. Chem. Soc.* **1985**, *107*, 7996.
(5) Dong, T.-Y.; Hendrickson, D. N.; Pierpont, C. G.; Moore, M. F. *J. Am. Chem. Soc.* **1986**, *108*, 963.
(6) Moore, M. F.; Wilson, S. R.; Cohn, M. J.; Dong, T.-Y.; Mueller-Westerhoff, U. T.; Hendrickson, D. N. *Inorg. Chem.* **1985**, *24*, 4559.
(7) Hendrickson, D. N.; Oh, S. M.; Dong, T.-Y.; Moore, M. F. *Comments Inorg. Chem.* **1985**, *4*, 329.
(8) Morrison, W. H., Jr.; Hendrickson, D. N. *Inorg. Chem.* **1975**, *14*, 2331.
(9) Motoyama, I.; Suto, K.; Katada, M.; Sano, M. *Chem. Lett.* **1983**, *1215*.
(10) Iijima, S.; Saida, R.; Motoyama, I.; Sano, H. *Bull. Chem. Soc. Jpn.* **1981**, *54*, 1375.
(11) Konno, M.; Hyodo, S.; Iijima, S. *Bull. Chem. Soc. Jpn.* **1982**, *55*, 2327.

0002-7863/86/1508-4423$01.50/0

one I–I bond in the I_3^- anion is shorter than the other. In short, the onset of charge oscillation in the I_3^- anion directly affects the *intra*molecular electron transfer in the mixed-valence cation. The presence of a phase transition involving electron transfer in biferrocenium triiodide has been established by variable-temperature heat-capacity measurements.[12]

Structural data for salts of trihalide ions such as I_3^-, $Br–I–Br^-$, etc., emphasize two important features. First, these trihalide ions are symmetrical in some salts[13] and unsymmetrical in others.[14] It is clearly not simply a question of the size of the cation. For example, in $[Ph_4As]I_3$ the I_3^- anions are well separated (shortest interanion I···I contact is 5.20 Å) and they are symmetrical.[13a] In the alkali salts of I_3^- there is a packing of the anions rather like that of I_2 molecules in crystalline iodine (shortest I···I contact distance of ~4.0 Å). Although Cs^+ is a large cation, the I_3^- anion in CsI_3 is unsymmetrical (I–I = 2.842 (2) and 3.038 (2) Å at 113 K),[13a,14a] whereas, in $KI_3·H_2O$ the I_3^- anion is symmetrical to within 0.005 Å.[13e] Second, the structural differences between trihalide ions have been attributed to the different environments of the terminal atoms in the crystals.

The effect of replacing I_3^- by Br_2I^- on the structure and conductivity of the conductor bis(ethylenedithio)tetrathiafulvalene (nicknamed "ET") has been noted very recently.[15] It was found that β-$(ET)_2(Br_2I)$ possesses a higher superconducting transition temperature (T_C = 2.7 K) than β-$(ET)_2(I_3)$. The dibromoiodate anion is linear, i.e., $Br–I–Br^-$, and on the basis of ionic radii, Br_2I^- is ~7% shorter than I_3^-. The smaller size of Br_2I^- is believed to lead to a decrease in the interstack S···S distances, thereby modifying the electrical properties.

In this paper the effect of replacing the I_3^- anion of biferrocenium triiodide by Br_2I^-, BrI_2, and PF_6^- is investigated. The dramatic changes in rates of *intra*molecular electron transfer that result are taken as further support for the presence of phase transitions. A qualitative model is advanced which delineates the nature of cooperative intermolecular interactions in the biferrocenium trihalide salts. The manner in which the trihalide anions micromodulate the intramolecular electron-transfer rate in the mixed-valence biferrocenium cation is described.

Experimental Section

Compound Preparation. A sample of biferrocene was prepared according to a literature method.[16] A solution of 0.1 M $HIBr_2$ was prepared by mixing 1.03 g of IBr and 0.81 mL of 50% HBr in a 50-mL volumetric flask and then diluting to the mark with methanol.[17] A solution of 0.1 M HI_2Br was prepared in the same fashion, using I_2 instead of IBr.

Biferrocenium dibromoiodate was prepared by dissolving biferrocene and a stoichiometric amount of *p*-benzoquinone in hexane–benzene (1:2) at 0 °C. To this solution a stoichiometric amount of 0.1 M $HIBr_2$ methanol solution was added dropwise with rapid stirring. The resulting solid was filtered, washed with a little cold benzene, and vacuum dried. Anal. Calcd for biferrocenium dibromoiodate ($C_{20}H_{18}Fe_2IBr_2$): C, 36.58; H, 2.76; Fe, 17.01. Found: C, 36.43; H, 2.60; Fe, 16.90.

Biferrocenium bromoiodoiodate was prepared in the same fashion as described for the dibromoiodate salt, using 0.1 M HI_2Br methanol solution instead of 0.1 M $HIBr_2$ solution. Anal. Calcd for biferrocenium I_2Br^- ($C_{20}H_{18}Fe_2BrI_2$): C, 34.13; H, 2.58; Fe, 15.87. Found: C, 34.10; H, 2.65; Fe, 15.71.

Biferrocenium PF_6^- was prepared by dissolving stoichiometric amounts of a biferrocene and *p*-benzoquinone in benzene. To this solution, a 0.1 M HPF_6 methanol solution was added dropwise with rapid stirring. The resulting solid was filtered, washed with a little benzene, and recrystallized from CH_2Cl_2. Anal. Calcd for biferrocenium PF_6^-: C, 46.64; H, 3.52; Fe, 21.69. Found: C, 47.35; H, 3.66; Fe, 21.03.

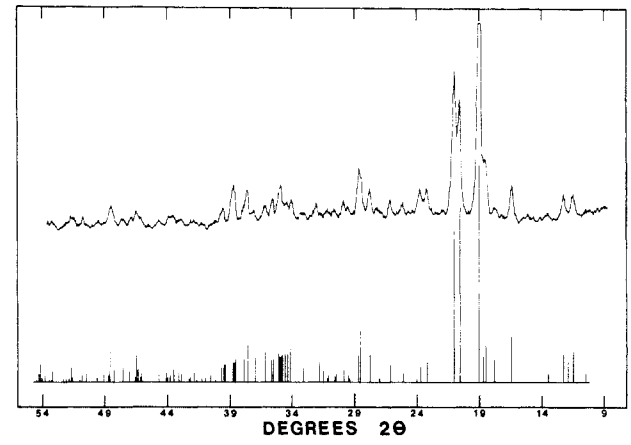

Figure 1. Room temperature powder X-ray diffraction pattern (top) for biferrocenium triiodide. The stick diagram resulted from a computer simulation employing the unit cell parameters and atomic positional parameters from the X-ray structure.[3,4]

Physical Methods. ^{57}Fe Mössbauer measurements were made on a constant-velocity instrument which has been described previously.[18] Mössbauer spectra were least-squares fit to Lorentzian line shapes with a previously documented computer program.[19] An attempt was made to report isomer shift data relative to that of iron foil at 300 K; however, second-order Doppler effects could only be estimated due to source temperature variability (the source was located within the exchange-gas cooled cryostat). It should be noted that the isomer shifts illustrated in the figures are plotted as experimentally obtained.

Variable-temperature X-band EPR spectra of powdered samples were run on a Bruker ER200 spectrometer equipped with an Oxford Instruments temperature controller. A calibrated copper–constantan thermocouple was used to determine the sample temperature. Samples were sealed in quartz tubes which had been pumped on a glass vacuum line.

Infrared spectra were obtained with a Nicolet Model MX-5 FT spectrometer. All samples were prepared as 13-mm KBr pellets with 2–5 mg of compound mixed well with 150 mg of KBr. A Spectrim closed-cycle refrigerator (Cryogenic Technology, Inc.) was used to cool the KBr pellets to ~50 K. The temperature of the KBr pellet holder was monitored with an iron-doped gold vs. chromel thermocouple.

X-ray powder diffraction patterns were obtained on a Norelco (Phillips Electronics Co.) powder diffractometer equipped with a copper X-ray tube and a graphite monochromator. A computer program was used to simulate powder patterns.[20] Trial-and-error computer-simulated patterns of biferrocenium dibromoiodate were obtained by using the atom coordinates[4] of biferrocenium triiodide, replacing the terminal iodine atoms with bromine atoms for trihalide anion, and then varying the unit-cell parameters. All of scattering factor constants are from the *International Tables for Crystallography*.[21]

Results and Discussion

Compound Preparation and Structure. Mixed-valence biferrocenium salts with Br_2I^-, I_2Br^-, and PF_6^- counterions were prepared as microcrystalline samples by immediate precipitation following the addition of a cooled solution of HBr_2I, HI_2Br, or HPF_6, respectively, to a cooled solution of biferrocene and *p*-benzoquinone. A large number of attempts were made by a variety of techniques, including low-temperature recrystallizations, slow diffusion of one solvent into another, and slow evaporations, to prepare X-ray quality crystals of the Br_2I^- and I_2Br^- salts. All attempts were unsuccessful apparently due to the fact that ions such as Br_2I^- dissociate in solution to give IBr which slowly oxidatively decomposes the biferrocene moiety. In fact, crystals which were isolated in the attempts to recrystallize the Br_2I^- salt

(12) Sorai, M.; Nishimori, A.; Dong, T.-Y.; Cohn, M. J.; Hendrickson, D. N., publication in preparation.
(13) (a) Runsink, J.; Swen-Walstra, S.; Migchelsen, T. *Acta Crystallogr.* **1972**, *B28*, 1331. (b) Soled, S.; Carpenter, G. B. *Acta Crystallogr.* **1973**, *B29*, 2556. (c) Migchelsen, T.; Vos, A. *Acta Crystallogr.* **1967**, *23*, 796. (d) General reference. (e) $KI_3·H_2O$ structural reference.
(14) Tasman, H. A.; Boswijk, K. H. *Acta Crystallogr.* **1955**, *8*, 59.
(15) (a) Whangbo, M.-H.; Williams, J. M.; Leung, P. C. W.; Beno, M. A.; Emge, T. J.; Wang, H. H. *Inorg. Chem.* **1985**, *24*, 3500; (b) Emge, T. J.; Wang, H. H.; Beno, M. A.; Leung, P. C. W.; Firestone, M. A.; Jenkins, H. C.; Cook, J. D.; Carlson, K. D.; Williams, J. M.; Venturini, E. L.; Azevedo, L. J.; Schirber, J. E. *Inorg. Chem.* **1985**, *24*, 1738 and references therein.
(16) Rausch, M. D. *J. Org. Chem.* **1961**, *26*, 1802.
(17) Klyachko, Y. A.; Larina, O. D. *Zavod. Lab.* **1964**, *30*, 930.
(18) Cohn, M. J.; Timken, M. D.; Hendrickson, D. N. *J. Am. Chem. Soc.* **1984**, *106*, 6683.
(19) Chrisman, B. L.; Tumolillo, T. A. *Comput. Phys. Commun.* **1971**, *2*, 322.
(20) Yvon, K.; Jeitschiko, W.; Parthe, E. *J. Appl. Cryst.* **1977**, *10*, 73.
(21) *International Tables for X-Ray Crystallography*; Kynoch Press: Birmingham, England, 1962; Vol. III.

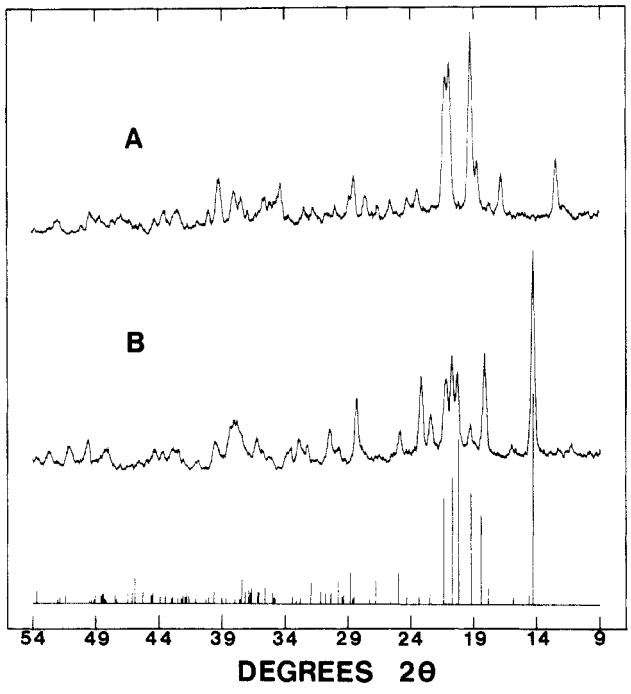

Figure 2. Room temperature powder X-ray diffraction patterns for biferrocenium I_2Br^- (A) and biferrocenium Br_2I^- (B). The stick diagram resulted from a trial-and-error simulation of the biferrocenium Br_2I^- pattern. See text for details.

were shown by a single-crystal X-ray structure to be biferrocenium tetrabromoferrate.[22] Obviously, the $FeBr_4^-$ anion resulted from the decomposition of the biferrocenium ion.

The power X-ray diffraction technique was employed to establish that the Br_2I^- and I_2Br^- biferrocenium salts have the same crystal structure as biferrocenium triiodide.[3,4] The room-temperature powder X-ray diffraction pattern of biferrocenium triiodide is shown in Figure 1, together with a pattern generated by a computer program utilizing the unit cell parameters and atomic positional parameters obtained from the single-crystal X-ray structure. Biferrocenium triiodide crystallizes in the $P\bar{1}$ space group at 296 K. As can be seen in Figure 1, the computer-generated simulation does agree well with the observed powder pattern.

In Figure 2 are shown the room temperature powder X-ray diffraction patterns for the biferrocenium Br_2I^- and I_2Br^- salts. It is immediately evident that biferrocenium I_2Br^- and biferrocenium I_3^- are isostructural. Although the powder pattern for the Br_2I^- salt looks somewhat different than those obtained for the I_3^- and I_2Br^- salts, there are some similarities. Relative to I_3^- and I_2Br^- patterns, the peaks for the Br_2I^- salt seemed to be shifted to larger 2θ values, which could indicate smaller dimensions in the unit cell. In an effort to understand the origin of the differences in powder patterns, a trial-and-error approach to simulate the powder pattern of the Br_2I^- salt was tried. In this simulation approach the atomic positional parameters[4] of biferrocenium triiodide were maintained throughout the calculations. The unit cell parameters of biferrocenium triiodide (see Table I) were varied to generate the "best" simulated pattern shown in the Figure 2. The final unit cell parameters used to give this "best" simulation are given in Table I. The unit cell parameters result from assuming the powder pattern of the Br_2I^- salt is smaller than those for either biferrocenium I_3^- or 1′,6′-di-*n*-propylbiferrocenium I_3^-, which is also of $P\bar{1}$ symmetry. In fact, we have found that the powder pattern for biferrocenium Br_2I^- looks similar to that[23] for 1′,6′-diethylbiferrocenium I_3^-. The packing arrangement in biferrocenium I_3^- consists of stepwise stacks of cations surrounded by stacks of anions. The above discussion, together with the fact

(22) Geib, S. J.; Rheingold, A. L.; Dong, T.-Y.; Hendrickson, D. N. *J. Organomet. Chem.*, in press.
(23) Dong, T.-Y.; Cohn, M. J.; Hendrickson, D. N., unpublished results.

Table I. Unit Cell Parameters[a]

	biferrocenium I_3^-	bi-ferrocenium Br_2I^-	1′,6′-di-*n*-propyl-biferrocenium I_3^-
a, Å	7.5779 (20)	6.5779	8.514 (8)
b, Å	8.4742 (14)	8.2742	8.5482 (5)
c, Å	9.5577 (21)	10.0577	10.9032 (13)
α, deg	112.619 (14)	115.488	89.546 (9)
β, deg	104.646 (20)	105.382	115.582 (9)
γ, deg	94.610 (19)	93.546	108.488 (7)

[a] Biferrocenium I_3^- crystallizes[4] at 296 K in the space group $P\bar{1}$. 1′,6′-Di-*n*-propylbiferrocenium I_3^- crystallizes[9] at 298 K in the space group $P\bar{1}$. The unit cell parameters for biferrocenium Br_2I^- were obtained by simulating the X-ray powder pattern assuming that this compound also crystallizes in the $P\bar{1}$ space group.

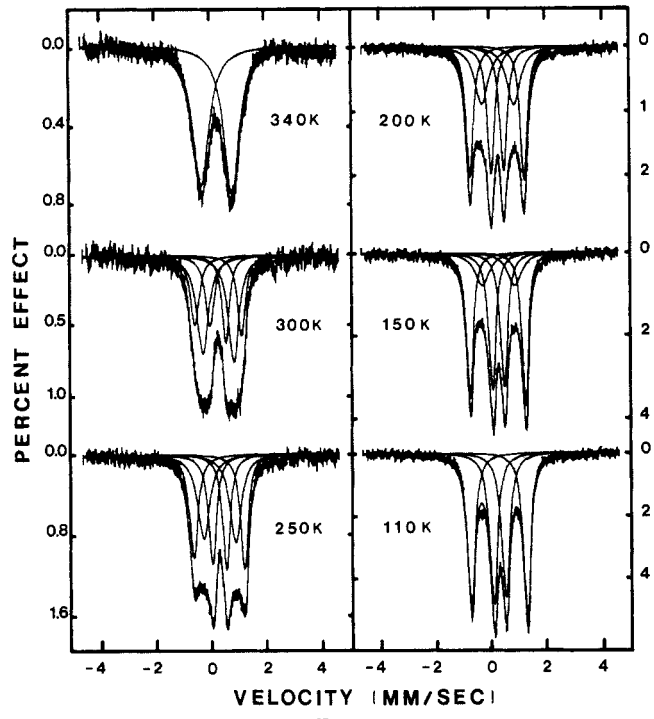

Figure 3. Variable-temperature ^{57}Fe Mössbauer spectra for a microcrystalline sample of biferrocenium I_2Br^-.

that the linear Br–I–Br^- anion is only 7 to 10% shorter than I–I–I^-, makes it probable that biferrocenium Br_2I^- crystallizes in $P\bar{1}$ and has a crystal packing arrangement not unlike the other two compounds. Very recent results[24] have shown that 1′,6′-dibenzylbiferrocenium I_3^- with its bulky substituents even has the same structure.

^{57}Fe Mössbauer Spectroscopy. Mössbauer spectra taken for a microcrystalline sample of biferrocenium I_2Br^- are shown in Figure 3. These six spectra were least-squares fit to Lorentzian line shapes to give the parameters given in Table II. The 110 K spectrum consists of two quadrupole-split doublets, one with a quadrupole splitting (ΔE_Q) of 2.021 (3) mm/s and the other with ΔE_Q = 0.441 (3) mm/s. Both doublets have the same spectral area. This pattern of two doublets is what is expected for a mixed-valence biferrocene which is valence trapped on the time scale of the ^{57}Fe Mössbauer experiment. In the least-squares fitting of the 150 K spectrum a third doublet with ΔE_Q = 1.173 (16) mm/s was added to get a good fit. This third doublet has the characteristics of a mixed-valence biferrocene with an *intra*molecular electron-transfer rate greater than $\sim 10^7$ s^{-1}. Increasing the temperature of biferrocenium I_2Br^- above 150 K leads to an increase in the relative intensity of this third doublet at the expense of the Fe^{II} and Fe^{III} doublets. As can be seen in Figure 3, at temperatures above ~340 K only the third doublet can be seen. The intramolecular electron transfer is occurring at a rate faster

(24) Pierpont, C. G.; Dong, T.-Y.; Hendrickson, D. N., unpublished results.

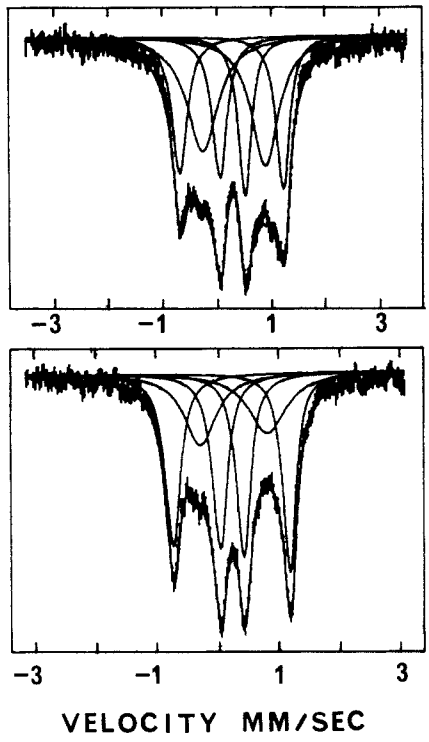

Figure 4. ^{57}Fe Mössbauer spectra taken at 300 K for two different samples of biferrocenium triiodide.

than can be sensed by the Mössbauer technique.

A comparison of the Mössbauer data reported[3,4] for biferrocenium I_3^- with those for the I_2Br^- salt indicates that these two compounds have similar Mössbauer temperature dependencies; however, everything is shifted to lower temperatures for the I_2Br^- salt. As is evident in Figure 3, the I_2Br^- salt gradually converts over a large temperature range (~200 deg) from localized to delocalized on the Mössbauer time scale. With biferrocenium I_3^- we have found that the range over which the spectrum changes (~70 deg) is smaller than that for the I_2Br^- salt and that this behavior is sample-history dependent.[23] For example, samples prepared by different crystallization approaches (evaporation, sudden precipitation, diffusion growth) give 300 K Mössbauer spectra with different amounts of localized and delocalized species (see Figure 4). The presence of a phase transition is indicated, which has been conclusively verified for biferrocenium I_3^- by heat-capacity and DSC measurements.[12] The variability in properties of these compounds from one analytically pure sample to another is a reflection of differences in the concentration of defect structure. The presence of defect structure such as crystallographic dislocations will tend to make a phase transition occur over a larger temperature range.

An amazing change in the Mössbauer characteristics results when the I_3^- anion of biferrocenium I_3^- is replaced by the Br–I–Br$^-$ anion. Biferrocenium dibromoiodate is localized at temperatures below ~150 K (see Figure 5), but increasing the temperature of the Br_2I^- salt up to 210 K gives a spectrum with but one "valence-delocalized" doublet. Mössbauer fitting parameters are given in Table II. The change from I_3^- to Br_2I^- leads to a change of ~150 K in the temperature at which the mixed-valence biferrocenium ion transfers electrons faster than the Mössbauer time scale. This dramatic change clearly indicates that the solid-state environment about the mixed-valence biferrocenium cation plays a crucial role in determining the rate of *intra*molecular electron transfer in this mixed-valence cation. A model which incorporates the possible *inter*molecular interactions in these mixed-valence biferrocenium salts is presented below.

In Figure 6 are shown variable-temperature Mössbauer spectra for a microcrystalline sample of biferrocenium PF_6^-. The Mössbauer behavior of this PF_6^- salt is quite different from those seen for the I_3^-, Br_2I^-, and I_2Br^- salts of the mixed-valence biferrocenium cation. Even without a computer fitting, it is clear

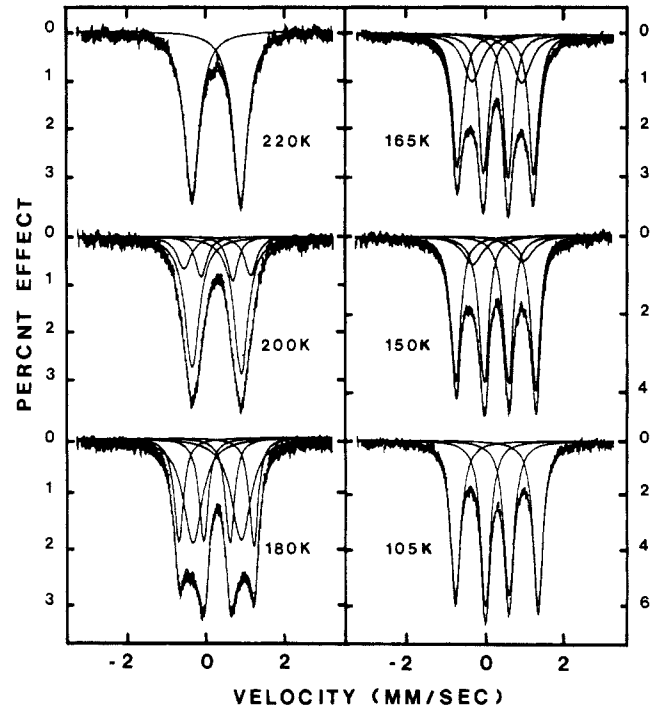

Figure 5. Variable-temperature ^{57}Fe Mössbauer spectra for a microcrystalline sample of biferrocenium Br_2I^-.

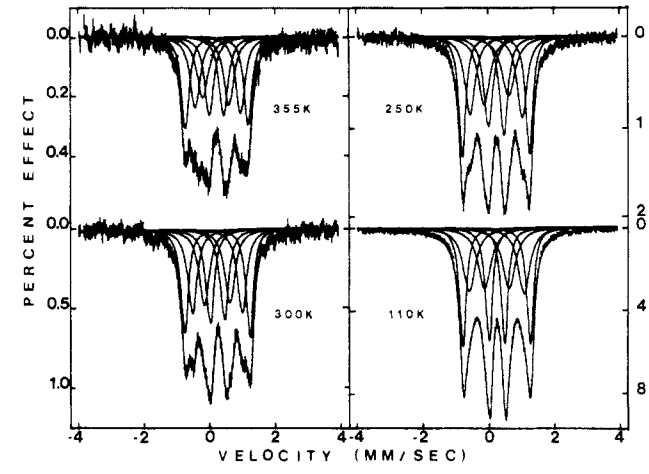

Figure 6. Variable-temperature ^{57}Fe Mössbauer spectra for a microcrystalline sample of biferrocenium PF_6^-.

from the 250 and 300 K spectra that there are at least six absorption peaks. However, it is not possible to fit these spectra by assuming that they consist of six lines that result from a superposition of a valence-localized pattern of two doublets of equal area (i.e., one Fe^{II} and one Fe^{III} doublet) and one other doublet. After trying a number of different fitting schemes, it was concluded that the spectra consist of a superposition of two valence-localized patterns, that is, eight Lorentzian line shapes where for each group of four lines the areas of each line are equal. The resulting least-squares fitting parameters are summarized in Table II. One four-line Fe^{II},Fe^{III} valence-localized pattern does not exhibit much of a temperature dependence. For this pattern at 110 K $\Delta E_Q(Fe^{II})$ is 2.063 (2) mm/s and $\Delta E_Q(Fe^{III})$ is 0.476 (3) mm/s, whereas these values change little to become 1.926 (9) and 0.440 (15) mm/s, respectively, at 355 K. The other four-line pattern does exhibit a temperature dependence which is evident from an inspection of the spectra. For this second pattern, $\Delta E_Q(Fe^{II})$ varies from 1.679 (5) to 1.392 (15) mm/s and $\Delta E_Q(Fe^{III})$ from 0.752 (6) to 0.802 (23) mm/s as the sample temperature is varied from 110 to 355 K. For this sample of biferrocenium PF_6^- the area ratio of the two four-line patterns was found to be close to 1:1; however, for a second microcrystalline sample we found that this ratio is appreciably different. It is likely that the four-line pattern

Table II. ^{57}Fe Mössbauer Least-Squares Fitting Parameters for Mixed-Valence Biferrocenium Salts[a]

counterion of biferrocenium salt	T, K	ΔE_Q, mm/s	δ, mm/s	Γ[b], mm/s	% deloc	% loc
I_3^-[c]	300	1.901 (4)	0.473 (2)	0.298 (11); 0.256 (10)	30.4	69.6
		1.097 (17)	0.526 (9)	0.626 (86); 0.742 (94)		
		0.383 (4)	0.481 (2)	0.292 (8); 0.256 (10)		
	300	1.898 (6)	0.501 (3)	0.324 (18); 0.278 (7)	46.6	53.4
		1.147 (10)	0.548 (5)	0.680 (60); 0.602 (57)		
		0.458 (6)	0.518 (3)	0.316 (14); 0.290 (15)		
I_2Br^-	340	1.115 (7)	0.525 (4)	0.706 (14); 0.662 (13)	100	0
	300	1.684 (27)	0.406 (13)	0.388 (56); 0.334 (53)	47.4	52.6
		1.117 (14)	0.503 (7)	0.500 (10); 0.460 (114)		
		0.568 (25)	0.494 (13)	0.386 (46); 0.310 (50)		
	250	1.836 (9)	0.496 (5)	0.362 (22); 0.326 (21)	37.0	63.0
		1.156 (10)	0.517 (5)	0.522 (74); 0.496 (72)		
		0.504 (9)	0.508 (4)	0.340 (18); 0.324 (18)		
	200	1.961 (4)	0.498 (2)	0.306 (11); 0.298 (10)	30.2	69.8
		1 160 (11)	0.532 (5)	0.590 (64); 0.590 (63)		
		0.455 (4)	0.515 (2)	0.312 (9); 0.320 (9)		
	150	2.005 (3)	0.495 (1)	0.284 (7); 0.269 (6)	19.8	80.2
		1.173 (16)	0.550 (8)	0.622 (85); 0.620 (83)		
		0.427 (3)	0.518 (1)	0.302 (6); 0.308 (6)		
	110	2.021 (3)	0.501 (1)	0.326 (4); 0.302 (4)	0.0	100.0
		0.441 (3)	0.523 (1)	0.332 (5); 0.348 (5)		
IBr_2^-	260	1.196 (4)	0.514 (2)	0.450 (7); 0.438 (7)	100	0
	220	1.208 (3)	0.524 (2)	0.510 (6); 0.490 (6)	100	0
	210	1.218 (3)	0.530 (2)	0.558 (6); 0.542 (6)	100	0
	200	1.823 (39)	0.508 (19)	0.426 (52); 0.388 (53)	68.0	32.0
		1.196 (5)	0.519 (3)	0.448 (41); 0.456 (36)		
		0.654 (36)	0.560 (18)	0.376 (50); 0.526 (44)		
	190	1.820 (22)	0.525 (11)	0.414 (34); 0.378 (34)	42.6	57.4
		1.201 (7)	0.528 (4)	0.468 (75); 0.456 (71)		
		0.680 (15)	0.543 (8)	0.372 (28); 0.396 (24)		
	180	1.905 (6)	0.515 (3)	0.310 (16); 0.306 (15)	40.4	59.6
		1.205 (11)	0.541 (6)	0.620 (56); 0.630 (52)		
		0.624 (5)	0.537 (3)	0.302 (14); 0.312 (14)		
	170	1.940 (3)	0.518 (2)	0.322 (10); 0.304 (9)	21.8	78.2
		1.188 (17)	0.561 (8)	0.600 (78); 0.680 (75)		
		0.606 (3)	0.539 (2)	0.310 (7); 0.320 (8)		
	150	1.992 (3)	0.521 (1)	0.348 (4); 0.324 (4)	0	100
		0.608 (2)	0.540 (1)	0.324 (4); 0.346 (4)		
	110	2.071 (2)	0.524 (1)	0.330 (4); 0.298 (4)	0	100
		0.572 (2)	0.546 (1)	0.292 (4); 0.320 (4)		
PF_6^-[d]	355	1.926 (9)	0.469 (4)	0.280 (13); 0.292 (14)		
		1.392 (15)	0.505 (8)	0.362 (26); 0.336 (20)		
		0.802 (23)	0.443 (12)	0.420 (43); 0.376 (31)		
		0.440 (15)	0.463 (7)	0.328 (22); 0.324 (24)		
	330	1.952 (7)	0.473 (4)	0.306 (12); 0.254 (9)		
		1.457 (12)	0.488 (6)	0.398 (22); 0.316 (13)		
		0.800 (13)	0.452 (6)	0.366 (22); 0.366 (20)		
		0.421 (9)	0.466 (4)	0.306 (14); 0.296 (14)		
	300	2.000 (6)	0.472 (3)	0.272 (9); 0.258 (8)		
		1.526 (9)	0.479 (4)	0.336 (13); 0.336 (13)		
		0.788 (13)	0.471 (6)	0.370 (19); 0.382 (21)		
		0.440 (9)	0.473 (4)	0.300 (13); 0.310 (14)		
	250	2.056 (3)	0.476 (2)	0.242 (5); 0.248 (5)		
		1.601 (7)	0.486 (3)	0.364 (10); 0.360 (10)		
		0.754 (14)	0.490 (7)	0.426 (20); 0.494 (23)		
		0.472 (8)	0.486 (4)	0.326 (12); 0.294 (9)		
	150	2.067 (2)	0.481 (1)	0.252 (4); 0.246 (3)		
		1.659 (5)	0.483 (2)	0.410 (8); 0.380 (7)		
		0.747 (7)	0.490 (4)	0.436 (12); 0.458 (12)		
		0.468 (4)	0.488 (2)	0.270 (5); 0.260 (4)		
	110	2.063 (2)	0.482 (1)	0.240 (3); 0.246 (3)		
		1.679 (5)	0.490 (2)	0.448 (8); 0.430 (8)		
		0.752 (6)	0.493 (3)	0.466 (11); 0.470 (11)		
		0.476 (3)	0.490 (1)	0.250 (3); 0.244 (3)		

[a] The estimated standard deviations in the least-significant figures are given in parentheses. [b] Full width at half-height taken from the least-squares fitting program. The width for the line at more negative velocity is listed first for each doublet. [c] Two different samples of biferrocenium triiodide were examined. Each was prepared by slowly adding a benzene solution of I_2 to a benzene solution of biferrocene over a period of 3 h. [d] Fitted into two sites which have 1:1 ratio.

is associated with biferrocenium cations which have an *intra*-molecular electron-transfer rate that is increasing with increasing temperature. The other four-line pattern reflects the presence of biferrocenium cations that remain valence localized on the Mössbauer time scale perhaps because of defect structure. It is unfortunate that the considerable efforts to grow a crystal of biferrocenium PF_6^- suitable for an X-ray structure determination were unsuccessful.

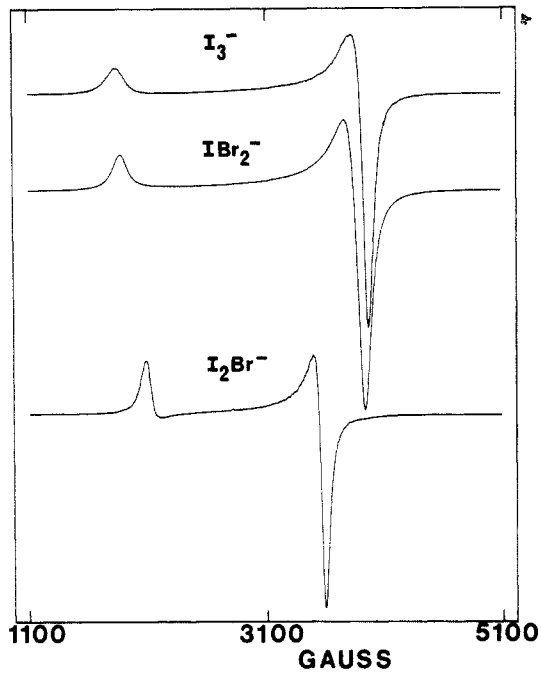

Figure 7. X-band EPR spectra for powdered samples of three biferrocenium salts at 4.2 K. The anions are indicated in the figure.

Table III. Electron Paramagnetic Resonance Data for Biferrocenium Salts[a]

counterion for biferrocenium salt	T (K)	$g_{\parallel}$	g_{HT}[b]	$g_{\perp}$	Δg[c]
I_3^-	4	3.66		1.73	1.93
I_2Br^-	3.9	3.23		1.90	1.33
Br_2I^-	4	3.60		1.75	1.85
	22	3.60		1.75	1.85
	60	3.57		1.76	1.81
PF_6^-	4	2.65	2.01	1.86	0.79
	90	2.64		2.00	
	140		2.07		

[a] EPR spectra were run for microcrystalline samples. [b] g_{HT} is calculated for the derivative-like feature which dominates the EPR spectrum at high temperatures. [c] This is the **g**-tensor anisotropy defined as $\Delta g = g_{\parallel} - g_{\perp}$.

Electron Paramagnetic Resonance. EPR has proven to be useful in the study of mixed-valence biferrocenes.[5,8] Localized Fe^{III} metallocenes generally give EPR signals only at low temperatures.[25] The orbital angular momentum in the ground state leads to appreciable **g**-tensor anisotropy, $\Delta g = g_{\parallel} - g_{\perp}$. Ferrocenium triiodide gives an axial 20 K EPR signal characterized by $g_{\parallel} = 4.35$ and $g_{\perp} = 1.26$ ($\Delta g = 3.09$). This **g**-tensor anisotropy can be reduced by a distortion of the Fe^{III} metallocene; a trimethylene strap between the two rings of a Fe^{III} metallocene tilts the two rings relative to each other and this explains why 1,1′-trimethyleneferrocenium hexafluorophosphate has $g_{\parallel} = 3.86$ and $g_{\perp} = 1.81$ with $\Delta g = 2.05$.[25] Mixed-valence biferrocenes that either have delocalized electronic structures with no potential-energy barrier for electron transfer or have an *intra*molecular electron-transfer rate in excess of the EPR time scale empirically have been found[5] to have Δg values less than ~0.8. This is a reflection of considerably reduced orbital angular momentum in the ground state which results from admixture of the $S = 0$ Fe^{II} description into the ground state.

X-band EPR spectra taken at 4.2 K for microcrystalline samples of the I_3^-, Br_2I^-, and I_2Br^- salts of the mixed-valence biferrocenium cation are shown in Figure 7. The g values evaluated from these and other EPR spectra are given in Table III. It is evident that the EPR spectra for the I_3^- and Br_2I^- salts are quite similar with

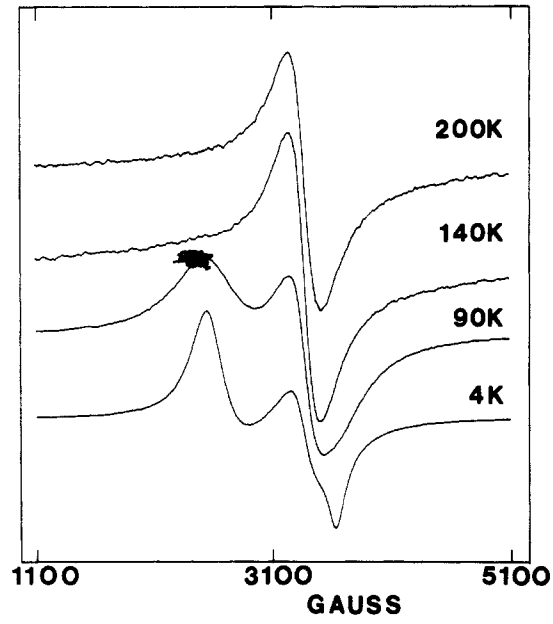

Figure 8. Variable-temperature X-band EPR spectra for a powdered sample of biferrocenium PF_6^-.

Δg values of 1.93 and 1.85, respectively, at 4 K. The I_2Br^- salt also exhibits an axial EPR spectrum; however, Δg (=1.33) is considerably reduced. There are significant conclusions that can be made on the basis of the spectrum for the I_2Br^- salt. First, it is clear that the I_2Br^- salt is not a mixture of I_3^- and Br_2I^- salts. Second, it is likely that neither does the I_2Br^- salt have a random distribution of I_3^-, I_2Br^-, Br_2I^-, etc., anions in one lattice nor is the I_2Br^- anion disordered in the crystals. Both of these situations would be expected to lead to more than one type of biferrocenium cation site in the lattice by virtue of different anion environments, and more than one EPR signal would have been expected. Support for the suggestion that the I_2Br^- anions are ordered in the lattice also can be seen in the fact that relatively intense peaks are evident in the powder X-ray diffraction pattern for this compound. There are only a few X-ray structures available for I_2Br^- salts. The I_2Br^- anions are ordered in CsI_2Br,[26] whereas, they are disordered in the organic conductor β-$(ET)_2I_2Br$,[15] where "ET" is bis(ethylenedithio)tetrathiafulvalene.

Since biferrocenium I_2Br^- is clearly isostructural with the I_3^- salt (vide supra), in the I_2Br^- salt there are stacks of biferrocenium cations surrounded by four stacks of I_2Br^- anions. Each mixed-valence cation has four neighboring I_2Br^- anions. If these four Br–I–I^- anions all have their bromine ends in the same direction, then it is conceivable that the biferrocenium cation in this salt would experience a greater low-symmetry crystal field than in the I_3^- and Br–I–Br^- salts. This could be the origin of the reduced Δg value.

A figure is available in the supplementary material to illustrate the temperature dependence of the EPR spectrum of biferrocenium Br_2I^-. As the temperature is increased above 4 K, the $g_{\parallel}$ and $g_{\perp}$ signals broaden such that above ~150 K no EPR signal is seen. This type of behavior has been seen for other mixed-valence biferrocenes.[5,8]

The EPR characteristics of biferrocenium PF_6^- are both intriguing and puzzling. Variable-temperature spectra are presented in Figure 8, where it can be seen that at 4 K three features can be seen at g values of 2.65, ~2.01, and 1.86. An increase in the temperature leads to the broadening and disappearance of the 2.65 and 1.86 signals. At 140 K only a single "derivative-like" signal with $g = 2.07$ remains. This signal basically remains unchanged up to 300 K ($g = 2.02$). Double integration of the EPR signal from 4 to 300 K shows that the signal intensity has a Curie-like behavior. The spectral area is inversely proportional to the absolute temperature in the 4–300 K range as you would expect for a simple

(25) Duggan, D. M.; Hendrickson, D. N. *Inorg. Chem.* **1975**, *14*, 955.

(26) Carpenter, G. B. *Acta Crystallogr.* **1966**, *20*, 330.

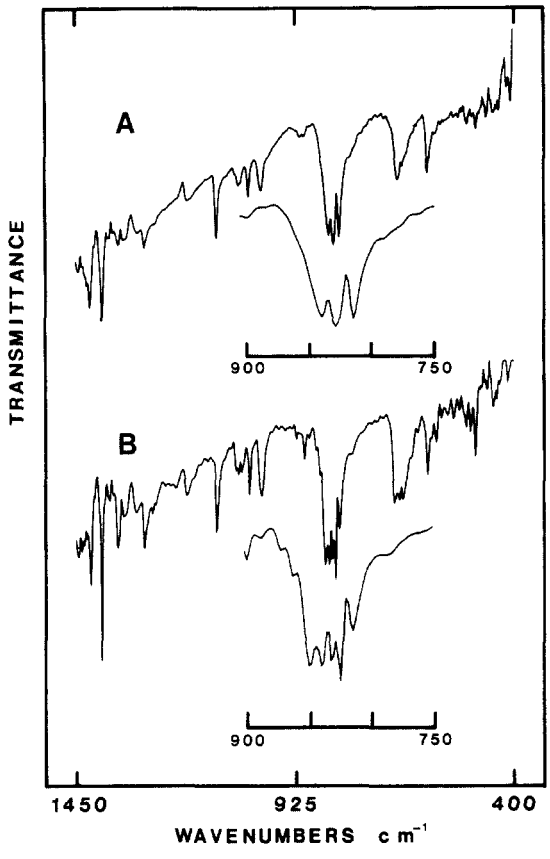

Figure 9. KBr-pellet FTIR spectra for biferrocenium I_2Br^- at two temperatures: 300 K (A); 50 K (B).

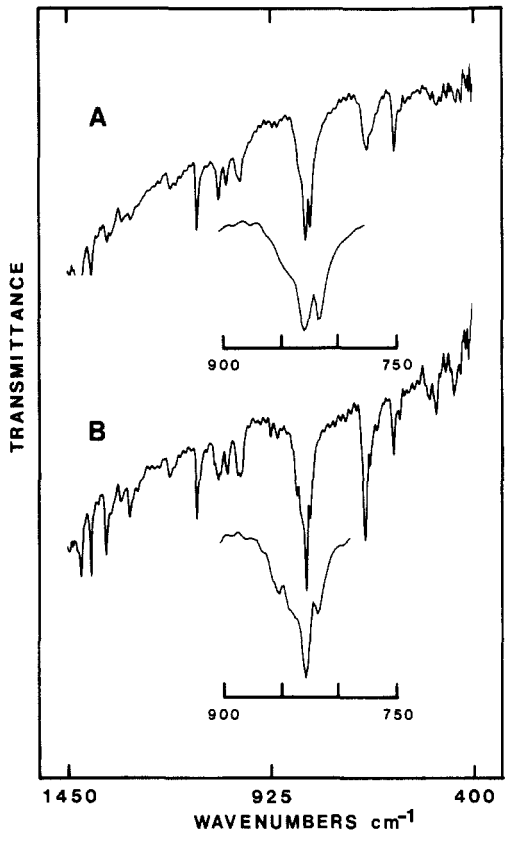

Figure 10. KBr-pellet FTIR spectra for biferrocenium Br_2I^- at two temperatures: 300 K (A); 50 K (B).

paramagnet. It is not clear what the origin of the $g = 2.07$ signal is. It is interesting to note that the g value is close to the average (=2.12) of the low-temperature $g_\parallel$ and $g_\perp$ signals. It does not seem that it is possible to assign the high-temperature $g = 2.02$ signal to mixed-valence biferrocenium cations which are involved in *intra*molecular electron transfer at a rate that is in excess of what the EPR technique can sense for two reasons. First, such a species with a fast rate of *intra*molecular electron transfer is also expected to give an axial EPR signal, not a single derivative-like feature.[5] Second, the Mössbauer data indicate that at 300 K the *intra*molecular electron transfer rate is no faster than $\sim 10^7$ s^{-1}. It would require a rate of $\sim 10^{10}$ s^{-1} to "average" two EPR signals separated by ~ 100 G.

The $g = 2.02$ signal for biferrocenium PF_6^- at 300 K could be due to a magnetic exchange interaction between paramagnetic Fe^{III} ions in neighboring biferrocenium cations. If the intercation magnetic exchange interaction ($\hat{H} = -2J\hat{S}_1 \cdot \hat{S}_2$) increased with increasing temperature such that $|J| > 0.01$ cm^{-1} above ~ 200 K, then the frequency ($>10^{10}$ s^{-1}) of electron exchange between Fe^{III} ions would exceed the EPR time scale. Depending on the relative orientation of magnetic axes between Fe^{III} ions on neighboring sites, such a rapid exchange of electrons could give an "average" g-value signal. Further work is needed to understand the origin of the $g = 2.02$ "average" signal.

Infrared Spectroscopy. As detailed in previous papers,[4,5,27] infrared spectroscopy has been employed to study mixed-valence biferrocenes. The perpendicular cyclopentadienyl C–H bending mode for a Fe^{II} metallocene typically occurs in a range from 805 to 815 cm^{-1}. The corresponding band for a Fe^{III} metallocene is found in the range of 850 to 860 cm^{-1}. Thus, a mixed-valence biferrocenium cation that has an appreciable potential energy barrier for *intra*molecular electron transfer and, consequently, does *not* have a completely delocalized electronic structure would be expected to show both Fe^{II} and Fe^{III} perpendicular C–H bending bands.

Variable-temperature (50–300 K) FTIR spectra were run for KBr pellets of the I_3^-, I_2Br^-, and Br_2I^- salts of the biferrocenium cation. Unoxidized biferrocene shows two strong C–H bending bands at 812 and 820 cm^{-1}. The spectra of the I_3^- and I_2Br^- biferrocenium salts look very similar in this region. Three bands at 816, 826 (with a shoulder at 833), and 840 cm^{-1} are seen at 300 K, and four bands at 826, 833, 839, and 849 cm^{-1} are seen at 50 K for biferrocenium I_3^-. In Figure 9 are given the 50 and 300 K spectra for the I_2Br^- salt (spectra for the I_3^- salt are available in the supplementary material). The I_2Br^- salt shows three bands at 816, 829, and 841 cm^{-1} at 300 K and four bands at 816, 831, 841, and 849 cm^{-1} in the 50 K spectrum (see Figure 9). It is clear that the IR data for the I_3^- and I_2Br^- salts conclusively indicate the presence of Fe^{II} and Fe^{III} moieties in both cases.

As can be seen in Figure 10, at first glance the perpendicular C–H bending region for biferrocenium Br_2I^- looks somewhat different than for the other two trihalide salts. However, after careful comparison of the spectra it can be concluded that the Br_2I^- spectral pattern is related to the other two. It appears that certain bands have experienced small shifts which produce some overlapping of bands. At 50 K the Br_2I^- salt exhibits bands at 817 and 826 cm^{-1} and a broad feature at 837 cm^{-1}. It does appear to have Fe^{II} and Fe^{III} moieties.

Micromodulation and the Electronic Localization–Delocalization Phase Transition. There are at least three types of observations that indicate the presence of a phase transition, the nature of which controls the rate of *intra*molecular electron transfer in mixed-valence biferrocenes: (1) sample-history dependence of Mössbauer spectra which show signals from both localized and delocalized species; (2) the anion dependence of electron-transfer rate for the biferrocenium cation; and (3) endothermic peaks seen in heat capacity and DSC data for biferrocenium triiodide. The most dramatic case illustrating the first type of observation can be drawn from our work[4] on 1′,6′-dibenzylbiferrocenium triiodide. A microcrystalline sample of this compound gives a 300 K Mössbauer spectrum which is dominantly that of a valence-localized species, i.e., one Fe^{II} and one Fe^{III} doublet. If the microcrystalline sample

(27) Kramer, J. A.; Hendrickson, D. N. *Inorg. Chem.* **1980**, *19*, 3330.

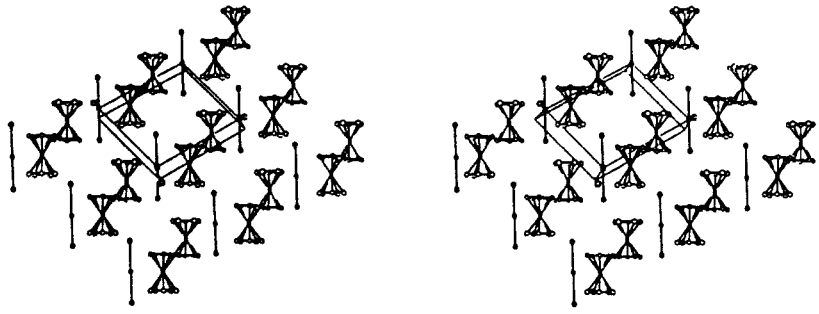

Figure 11. Stereoview of the packing arrangement in biferrocenium triiodide.

is dissolved in CH_2Cl_2 and hexane is allowed to diffuse into the CH_2Cl_2 solution such that X-ray structure quality crystals grow, these crystals will give a 300 K Mössbauer spectrum which consists only of one average-valence doublet. The anion dependence of electron transfer in the case of the biferrocenium cation was described above. Finally, the third type of observation has been thoroughly examined for biferrocenium triiodide. This compound is now known[4] to convert from Mössbauer-localized at ~300 K to Mössbauer-delocalized at ~357 K. A DSC examination of several samples of biferrocenium triiodide has revealed an endothermic peak in this temperature range. Furthermore, the heat capacity at constant pressure (C_P) has been measured from 13 to 360 K for a 11-g sample of biferrocenium triiodide.[12] At this time, it is only important to note that a sharp endothermic peak was seen at 328 K with two broader features at 312 and 346 K. A detailed analysis of these results will be presented later.[12]

A careful examination of Figure 11, which shows a stereoview of the packing arrangement in biferrocenium triiodide, points to two *inter*molecular interactions that could be important in an electronic localization–delocalization phase transition. There are step-like stacks of biferrocenium cations developing approximately along the ⟨011⟩ direction. Cation–cation interactions develop as the result of the appreciable cyclopentadienyl–cyclopentadienyl contact between two cations. The Cp–Cp interplanar distance is only 3.4 Å. The second type of intermolecular interaction that could be important occurs between a mixed-valence cation and its nearest-neighbor anions. As mentioned above, each I_3^- ion is in essence a mixed-valence species. It can oscillate between two different forms, which in their limiting views can be represented as $I_A—I_B\cdots I_C^-$ and $I_A^-\cdots I_B—I_C$. This oscillation in the inhomogeneous charge distribution in the neighboring I_3^- anions will impact on the rate of electron transfer in the mixed-valence cation.

It is appropriate to note that not only do the I_3^-, I_2Br^-, and Br_2I^- salts of the biferrocenium cation have the solid-state structure pictured in Figure 1 but also the 1′,6′-di-X-substituted biferrocenium triiodides where X can be ethyl, *n*-propyl,[11] or benzyl[24] are isostructural ($P\bar{1}$ space group). Of course, from one compound to another the extent of Cp–Cp overlap between cations in the step-like stacks, as well the magnitude of interaction between cation and neighboring anions, will change. In fact, from the X-ray structure[4] of 1′,6′-di-*n*-butylfiberrocenium triiodide ($P2_1/C$ space group) it is clear that there is no Cp–Cp overlap between cations in this compound. The bulkiness of the *n*-butyl substituents has apparently led to the mixed-valence cations sliding away from each other. If this compound is to be viewed as consisting of step-like stacks of cations, then the interaction between cations is transmitted via one *n*-butyl group of one cation contacting the "top" of one cyclopentadienyl group fo the next mixed-valence cation. However, this type of contact could still have the same effect as the Cp–Cp contact in determining the level of cooperativity in a given phase transition.

A qualitative description of the manner in which the above two intermolecular interactions lead to an electronic localization–delocalization phase transition can be given. First, consider the cation–cation interaction that develops down the step-like stack of mixed-valence cations. When an *intra*molecular electron transfer occurs in one cation, the two Cp rings bound to the Fe^{II} ion move away from the metal to assume the larger dimensions appropriate for a $(Cp)_2Fe^{III}$ moiety. At the same time the dimensions of the $(Cp)_2Fe^{III}$ moiety contract to those of a $(Cp)_2Fe^{II}$ species. The overall change can be represented schematically (overemphasized) as follows:

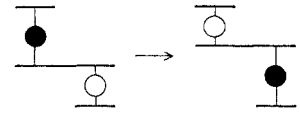

As detailed in the PKS vibronic model, a plot of the potential energy of such a mixed-valence complex as a function of this out-of-phase combination of Cp–Fe–Cp breathing modes ($Q = Q_A - Q_B$) on the two halves of the biferrocenium cation leads to the typical double-well potential energy diagram pictured in Figure 12A. Both the Coulomb interaction and the steric repulsion between two adjacent cations stabilize the state where each electron is localized on the equivalent iron ion in the two cations, that is, they stabilize the molecular distortion in the common direction as shown in Figure 13A. The cooperative electron localization or molecular distortion may be induced by the intercation interactions. Then, the stack of cations is in such an ordered localization or distortion state as indicated in Figure 13A: it has been found in 1′,6′-di-*n*-propylbiferrocenium triiodide[11] that ferrocene- and ferrocenium-like units are crystallographically discernible in the cation at 110 K. The potential energy curve for a cation becomes asymmetric in the ordered localization state as shown in Figure 12B. The energy difference W between the two potential wells for a single molecule is proportional to the cation–cation interaction, E_{CC}.[28] The potential energy barrier height for a single molecule is defined as ΔE_B in Figure 12.

Three limiting cases develop for different relative values of ΔE_B and E_{CC}. When $\Delta E_B \gg E_{CC}$ and the ΔE_B barrier is too high for a mixed-valence cation to transfer between the two potential wells, each stack of cations will remain fixed in an ordered arrangement at low temperature ($k_BT < E_{CC}$) as indicated in Figure 13A. At

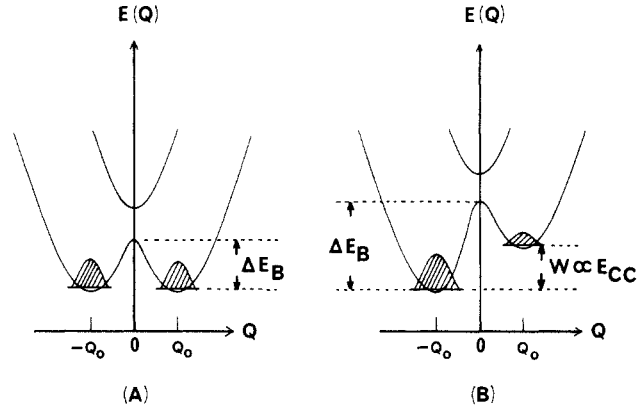

Figure 12. Potential energy plotted as a function of the out-of-phase combination of the two symmetric metal–ligand breathing vibrational modes on the two halves of a binuclear mixed-valence species. Diagram A is for a symmetric mixed-valence complex in the absence of environmental effects. Diagram B results if the environment about the binuclear mixed-valence complex is asymmetric.

(28) Kambara, T.; Hendrickson, D. N.; Dong. T.-Y.; Cohn, M. J., publication in preparation.

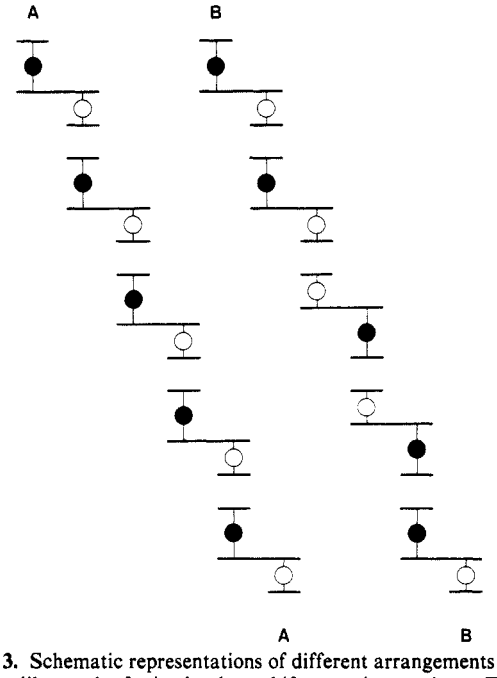

Figure 13. Schematic representations of different arrangements possible for a step-like stack of mixed-valence biferrocenium cations. Edgewise views of the cyclopentadiene and fulvalenide rings are shown. The Fe^{II} metallocene unit is indicated to have a smaller ring-to-ring distance than the Fe^{III} metallocene unit. Drawing A shows an ordered stack of electronically localized biferrocenium cations. Drawing B shows a disordered stack of localized biferrocenium cations.

the low temperature each cation occupies only the lower potential well in Figure 12B. As the temperature is increased, the thermal energy k_BT may exceed E_{CC} ($\propto W$) and many cations may occupy the higher potential well. Then, the cooperative order of the electron localization in the stack of cations disappears and the potential energy curve becomes symmetric. The electronically localized molecules in the stack will become disordered as indicated schematically in Figure 13B.

If ΔE_B and E_{CC} are of comparable magnitude, then certain mixed-valence cations in a stack can become activated and transfer an electron. Thermal energy is focused in a few mixed-valence cations as a result of the appreciable intermolecular interaction, and these few cations transfer an electron and adjust their molecular dimensions. It is possible that the activated cations will function as a soliton, that is, a boundary region between two domains which possess the opposite sense of valence localization. Regions (solitons) in the stack of cations will appear where cations have equal geometries on the two metallocene moieties. A schematic representation of a soliton between two localized domains is shown in Figure 14A. The soliton is comprised of a number of cations in various degrees of distortion intermediate between Q_0 and $-Q_0$ (see Figure 12). These solitons would be moving down (and up) the cation stacks at some characteristic velocity.

The dynamical equation for the soliton in a stack of mixed-valence biferrocenium cations[28] is qualitatively equivalent to the equations for ferroelectrics[29] and for polyacetylene,[30] but the detailed property of the soliton is different from the latter cases. When the temperature is increased and the thermal energy k_BT approaches to E_{CC} ($\sim\Delta E_B$), rapid electron transfer may occur in a large fraction of the mixed-valence cations in the stack. The concentration of solitons has increased to the point that solitons are frequently moving past a given cation. Consequently, each cation is rapidly inconverting between the two vibronic states. When the temperature exceeds E_{CC}/k_B, the order of electron localization in the stack disappears, that is, there is no domain. The electron in each cation is delocalized and every cation has

(29) Krumhansl, J. A.; Schrieffer, J. R. *Phys. Rev. B* **1975**, *11*, 3535.
(30) Su, W. P.; Schrieffer, J. R.; Heeger, A. J. *Phys. Rev. B* **1980**, *22*, 2099.

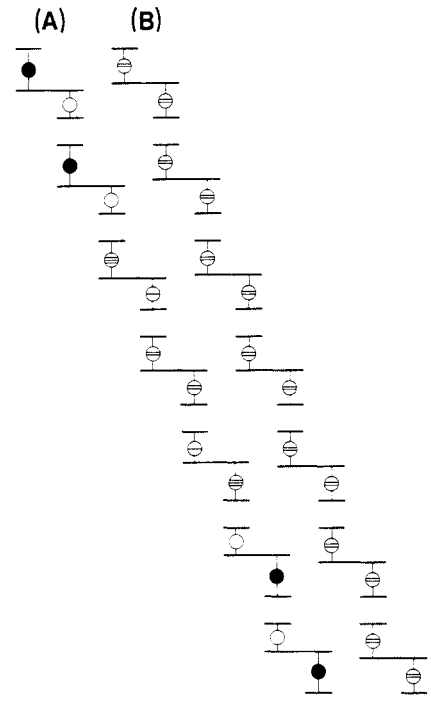

Figure 14. Drawing A shows a soliton between two ordered regions of electronically localized biferrocenium cations. Drawing B shows a stack of electronically delocalized biferrocenium cations.

equal geometry on the two metallocene moieties as indicated in Figure 14B.

In the third limiting case when $\Delta E_B \ll E_{CC}$, each stack is ordered at a low temperature of $k_BT \ll E_{CC}$, even though the thermal energy is such that an individual isolated molecule would be able to go over the barrier ΔE_B. Since nonlinear energy arising from the double-well potential of an individual cation is quite small compared with the linear intercation interaction energy E_{CC}, there is no soliton in the present case. As the temperature is increased and the thermal energy k_BT exceeds E_{CC}, the order in electron localization disappears in the stack and the electron in each cation is completely delocalized as indicated in Figure 14B.

If there are only interactions between cations in one stack, there will not be a phase transition if the system is one dimensional. From the previous sections the dramatic effect of changing the anion upon the intramolecular electron-transfer rate has been clearly established. In biferrocenium triiodide[4] the shortest Fe···I distances between the iron ions and the terminal atoms of the I_3^- anion are 5.2–5.7 Å. It is very likely that asymmetry in charge distribution which develops in the triiodide anion will directly affect the potential energy diagram of the mixed-valence biferrocenium cation. Consider the positioning of two asymmetric I_3^- anions next to a biferrocenium cation, viz.:

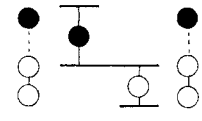

If the shaded atom of the I_3^- is further from the central iodine atom and carries more negative charge than the other terminal iodine atom, there will be valence localization in the mixed-valence cation. The potential energy diagram of the mixed-valence cation is made to be asymmetric as indicated in Figure 12B. The Coulomb interaction with two anions which have such an asymmetric charge distribution will introduce a large zero-point energy difference between the two vibronic states of the mixed-valence cation. The ironic point is that the I_3^- anion could be a mixed-valence species as well. In the absence of any environmental effects, the I_3^- anion has a symmetric double-well potential energy diagram as in Figure 12A. If the cation environment about a I_3^- anion is not symmetric, the I_3^- anion will have an asymmetric potential energy diagram as in Figure 12B. It has been observed

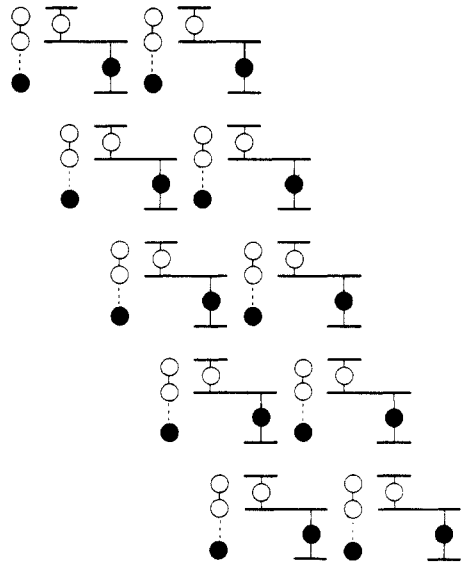

Figure 15. Schematic representation of a two-dimensionally-ordered section of biferrocenium triiodide.

in 1′,6′-di-*n*-propylbiferrocenium triiodide[11] at 110 K that bond distances of I(1)–I(2) and I(1)–I(3) are different in each I_3^- anion.

With the type of cation–cation and cation–anion interactions described above, it is possible to understand why at low temperature there could be three-dimensional order in a crystallite of biferrocenium triiodide. A schematic representation of a two-dimensionally ordered section of biferrocenium triiodide is shown in Figure 15. The exact nature of a phase transition which will occur as the temperature of such an ordered phase is increased will depend on the relative magnitudes of the cation–cation and cation–anion interactions as well as other factors such as defect structure.

In the context of the above model it is understandable how the change from I_3^- to Br_2I^- for the counterion could lead to a change of ~150 deg in the temperature at which the mixed-valence biferrocenium cation transfers faster than the Mössbauer time scale. The Br–I bonding interaction in Br_2I^- is weaker than the I–I bonding interaction in I_3^-, and as a consequence ΔE_B (Figure 12A) would be smaller for Br_2I^- than for I_3^-. Thus, the Br_2I^- anion would begin to oscillate between its two forms at lower temperatures than the I_3^- anion if the cation–anion interaction is greater than or comparable to the cation–cation interaction. This anion charge oscillation would lead to the onset of *intra*molecular electron transfer in the biferrocenium cation at a lower temperature for the Br_2I^- salt than for the I_3^- salt.

The sample-history dependence of the Mössbauer signals and DSC thermal effects seen for these mixed-valence biferrocenium salts are also explicable in terms of the above discussion. Crystalline samples prepared in different experiments can have appreciably different defect concentrations. Defects exist generally in profusion in crystalline material. There can be point defects such as vacancies or isolated impurities, line defects such as crystallographic dislocations, and a variety of surface defects. These defect sites serve as preferred sites of nucleation of critical size nuclei of a minority phase within a majority phase. The critical size nuclei grow at some rate eventually to become domains of the majority phase. If a minority-phase nucleus encounters defect structure as it is growing in size, the activation energy for further growth will be appreciably increased. It is understandable why the properties of a microcrystalline sample of a mixed-valence biferrocenium salt could be quite different from those of a more crystalline sample.

Acknowledgment. We are grateful for support from National Institutes of Health (Grant HL13652).

Registry No. Biferrocenium I_3^-, 39470-17-2; biferrocenium I_3Br^-, 102649-03-6; biferrocenium IBr_2^-, 99874-85-8; biferrocenium PF_6^-, 70282-49-4; biferrocene, 1287-38-3.

Supplementary Material Available: Figure 1, temperature dependence of X-band EPR spectrum for a powdered sample of biferrocenium Br_2I^-, and Figure 2, KBr pellet FTIR spectra for biferrocene and biferrocenium triiodide (2 pages). Ordering information is given an any current masthead page.